Structure of Liquid Chloroform as Investigated by Energy-Dispersive X-Ray Diffraction

Akinori Takahashi,# Yohko F. Yano, and Takao Iijima*

Department of Chemistry, Gakushuin University, Mejiro, Toshima-ku, Tokyo 171-8588

(Received March 9, 1998)

The structure of liquid chloroform has been investigated by energy-dispersive X-ray diffraction. For the stability of the sample thickness, even for a volatile liquid, a glass capillary tube has been used as a sample container. The intensity function has been accounted for by a bcc (body-centered cubic)-like local lattice structure model with a lattice constant of 6.24 Å. However, it has been necessary to replace a fraction (34%) of the nearest neighbors by super-near configurations in which molecules are rather tightly correlated. The correlation is, however, rapidly lost as the distance between molecules increases, and the long range structure is characterized by a large Prins parameter. The structure of liquid chloroform is much less ordered than that of carbon tetrachloride.

The structure of several molecular liquids was investigated by X-ray diffraction by one of the present authors (T. I.) and co-workers using an energy-dispersive method.[1] In these studies the structure of a liquid was characterized by the local lattice structure,[2] which represents the short-range ordered structure around a molecule and by the Prins parameter, which indicates how rapidly the local lattice becomes diffuse as the distance from the molecule increases.[3] As an extension of these previous studies, the structure of liquid chloroform (trichloromethane) was investigated in the present study.

In the previous studies, liquid samples were held between two Myler sheets as a thin layer.[4] Although this sample holder worked satisfactorily, it was desired to have a better device in order to secure the stability of the sample thickness, especially for a volatile liquid. In the present study a sample holder for use of a glass capillary tube was made. The use of a capillary tube inevitably led to a more complicated procedure of absorption correction for a cylindrical sample, as worked out by Paalman and Pings.[5] Fortunately, it posed no serious problem, since necessary numerical integrations can be easily performed by today's computing facilities.

Bertagnolli et al. obtained neutron diffraction results for $CDCl_3$ in natural isotopic composition and for enriched $CD^{35}Cl_3$ and $CD^{37}Cl_3$; together with X-ray diffraction results they extracted four coefficients of the invariant expansion of the molecular pair-correlation function of liquid chloroform at 20 °C.[6—8] Their conclusions were that there are six nearest neighbors at 4.8 Å, with an antiparallel alignment of the molecular C_3-axes, and that a stronger parallel alignment of the molecular C_3-axis along the center–center line must be present. They did not suggest any local lattice structure.

Present address: Hitachi Soft-Ware Engineering Co., Ltd., Kinkou-cho 9-12, Kanagawa-ku, Yokohama 221-0056.

Experimental

The diffraction intensities were measured by the energy-dispersive method at room temperature. A diffractometer with a horizontal scattering plane was used. The scattered photons were detected by means of a pure Ge SSD (solid state detector) backed up by a multichannel pulse-height analyzer. Except for the sample holder and minor modifications in the slit system, the diffractometer was similar to that reported by Murata and Nishikawa.[9] The optical setup is depicted in Fig. 1. Data were collected at scattering angles 2θ = 8, 15, 25, 45, and 70° at room temperature. Three sets of intensities, namely those obtained with the sample, with an empty capillary tube in the sample holder and without a capillary tube, were measured at each scattering angle. The intensity function was obtained for the range of 0.6—20 $Å^{-1}$ in the scattering parameter s ($s = (4\pi/\lambda)\sin\theta$; λ is the X-ray wavelength, and θ is the half-scattering angle). A sealed-off tube with a tungsten target was operated at 5 mA and 47.5 kV. The accumulation time was 12000 to 80000 s.

Sample Holder. A sample holder made of brass is shown in Fig. 2, which was fixed at the center of the goniometer. A glass capillary tube with a 1 mm inner diameter and a 0.01 mm

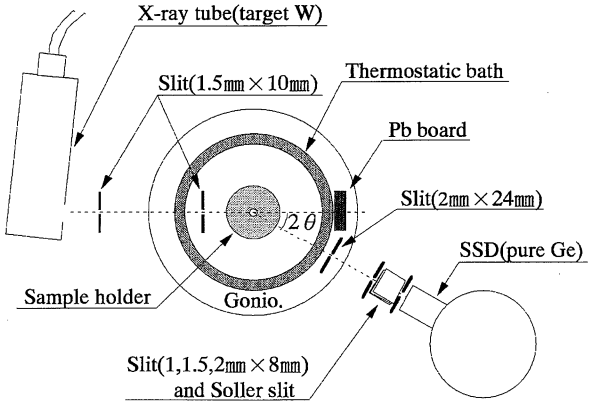

Fig. 1. Optical setup of the energy-dispersive diffractometer. Thermostatic air-bath was not used in the present study.

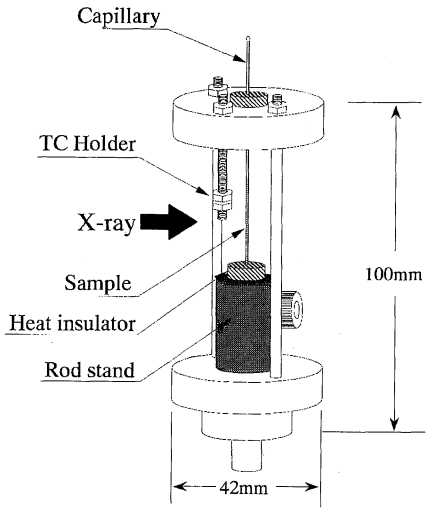

Fig. 2. Sample holder for use of a capillary tube as a container.

thickness (Lindemann glass MARK-TUBE from Hilgenberg) was held vertically by means of heat-insulating disks made of Duracon (polyacetal). The bolt, nuts and washers for the thermocouple holder were made of polycarbonate for heat insulation. The top opening of the capillary tube was loosely stopped to allow the vapor of the sample to escape. For measurements at other than room temperature the sample holder can be placed in a thermostatic air-bath with windows of Kapton film.

The absorption factor for $2\theta = 0°$ was experimentally measured in the setup shown in Fig. 3. X-Rays scattered by an empty capillary tube were used as the incident beam, which had a rather uniform energy spectrum. Another capillary tube with or without a sample was placed in the slit just before the detector. The narrow opening between the tube and the slit-edge was covered with a thin sheet of lead.

Analysis

The procedure for reducing the accumulated X-ray counts to the coherent intensities per molecule was the same as that reported previously,[10] except for an absorption correction. Paalman and Pings formulated the computational method for the absorption factors for a cylindrical sample in an annular cell.[5] They used the radial coordinates and skillfully reduced

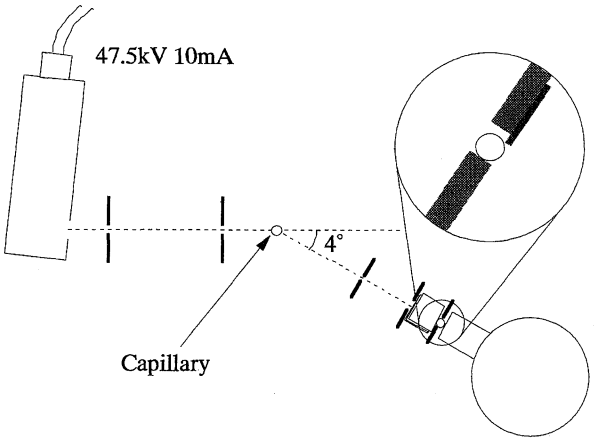

Fig. 3. Setup for the measurement of the absorption factor at $2\theta = 0°$.

the number of terms to be summed up without any loss of numerical accuracy. For today's computing facilities, however, it is not necessarily a primary concern to reduce the computing load. Thus, in the present study, the equations given in Ref. 5 were not used, but a more straightforward method formulated by using the rectangular coordinates was adopted. The numerical integrations were carried out by employing as many grid-points as necessary.

The absorption factor (A) for the cylindrical sample is given as an average over the scattering position (a,b) within the circle of the section with radius R by

$$A(E,\theta) = \int\int \exp\{-\mu(E)l(2\theta)\}\mathrm{d}a\mathrm{d}b/\pi R^2, \qquad (1)$$

where $\mu(E)$ is the X-ray energy-dependent linear-absorption coefficient and $l(2\theta)$ is the path length for the scattering point (a,b), given by

$$l(2\theta)=\frac{b\tan 2\theta - a - \{R^2(1+\tan^2 2\theta)-(b+a\tan 2\theta)^2\}^{1/2}}{(1+\tan^2 2\theta)^{1/2}} + (R^2-b^2)^{1/2} - a, \qquad (2)$$

(see Fig. 4). An equation equivalent to Eq. 2 was given by Bond for a different coordinate system.[11] The linear absorption coefficients ($\mu(E)$) were calculated from the mass absorption coefficients in the table[12] and the densities. Integration of Eq. 1 was actually performed by a numerical summation using 7825 scattering points (grid-points with $0.02R$) intervals). A sufficient integration convergence was confirmed for more than 5000 points. Exactly speaking, $A(E,\theta)$ is a transmission factor; however, since it has been traditionally called an absorption factor, it is called such in this paper.

The scattering process depicted in Fig. 4 may be said to be that scattered by the sample and absorbed by the sample, and the corresponding absorption factor may be denoted as $A_{s,s}$. The measurements carried out in the present study involve other scattering processes also, such as that scattered by the cell and absorbed by the sample and so on, as depicted in Fig. 5. The absorption factors for these processes were also calculated similarly. (The numerical values of $A_{c,c}$ are unnecessary in the analysis.) In addition to those shown in Fig. 4, the absorption factors $A_{a,a}$, $A_{s,a}$, $A_{c,a}$, etc., where the subscript a stands for air, must be considered. The numerical values are, however, unnecessary.

The scattering intensities actually measured are due to a combined process in which X-rays scattered by the sample are absorbed by the sample, the cell and air at the same

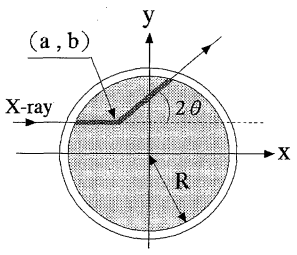

Fig. 4. Coordinate system for calculating the path lengths.

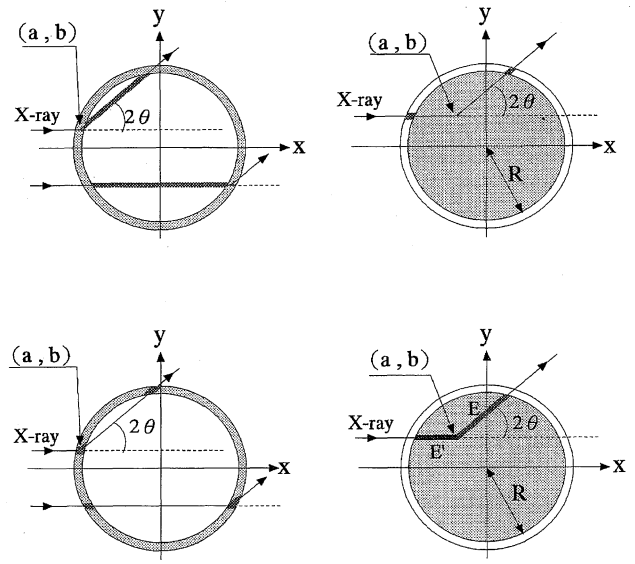

Fig. 5. Various scattering processes.
The absorption factors for these processes are denoted, from top left to right, as $A_{c,s}$, and $A_{s,c}$, and from bottom left to right, as $A_{c,c}$ and $A_{s,s,inc}$.

time. The absorption factor may be denoted as $A_{s,c+s+a}$, which was, however, approximated by the product $A_{s,c}A_{s,s}A_{s,a}$ in the present study.

The absorption coefficients of the cell (capillary tube) were calculated based on the composition of the main components in weight percentages: SiO_2 69, Na_2O 17, CaO 7, and others 7, and the linear absorption coefficients for Cu $K\alpha$ 97.4 cm^{-1} and for Mo $K\alpha$ 10.5 cm^{-1}.[13] Since the unknown component "others" had to be ignored, the weight percentages of the main components were shifted to SiO_2, 74.2; Na_2O, 18.3; and CaO, 7.5% in the calculation.

The experimentally measured absorption factors of water, ethylene glycol and chloroform for $2\theta = 0°$ were compared with the calculated values. The agreement was satisfactory for water and ethylene glycol, but a systematic deviation in the low energy region was observed for chloroform as shown in Fig. 6. Although the tabulated mass-absorption coefficients for chlorine may have some systematic errors,[9] they were used in the analysis, and data at energies less than 16 keV were discarded.

The scattering intensity from the sample at a scattering angle of 2θ is the basis of structure analysis. The theoretical expression for this quantity is given by[1,10]

$$I_s(E,\theta) = k\left\{I_{coh}(E,\theta) + \frac{(E'/E)A_{inc}(E,E',\theta)P(E',\theta)I_p(E')I_{inc}(E',\theta)}{A_{coh}(E,\theta)P(E,\theta)I_p(E)}\right\}, \quad (3)$$

where $I_{coh}(E,\theta)$ and $I_{inc}(E',\theta)$ are the coherent and incoherent cross section of the sample, respectively, (often called the intensity per molecule), $A_{coh}(E,\theta)$ the absorption factor $A_{s,s}$, $A_{inc}(E,E',\theta)$ the absorption factor $A_{s,s,inc}$, $P(E,\theta)$ the polarization factor, and $I_p(E)$ is the energy spectrum of the

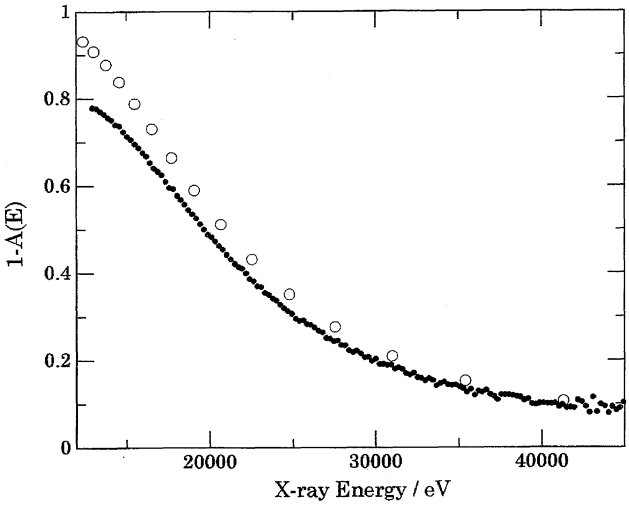

Fig. 6. Comparison of experimental (dots) and calculated (circle) $1-A_{s,s}(E)$ for chloroform at $2\theta = 0°$.

primary beam; E' is the primary photon energy that is to be reduced to E by the Compton shift. It should be noted that the factor (E'/E) is the product of the recoil factor (E/E') and the bandwidth ratio $(E'/E)^2$, as discussed in Ref. 10. The double scattering is neglected because its contribution is only a few percentage and shows a rather uniform dependence on X-ray energy even in the case of carbon tetrachloride.[10]

After making corrections for the slit width, escape and polarization,[10] and normalization by the accumulation time, three sets of experimentally measured intensities (I_s^{obs} obtained with the sample, I_c^{obs} with an empty capillary tube, and I_a^{obs} without the sample holder (with air only)) were related to I_s given by Eq. 3, and the corresponding quantities, I_c and I_a, for the capillary tube and air, respectively, as the following,

$$I_s^{obs} = (A_{s,s}A_{s,c}A_{s,a}I_s + A_{c,s}A_{c,c}A_{c,a}I_c + \beta A_{a,s}A_{a,c}A_{a,a}I_a + (1-\beta)A_{a,a}I_a)\cdot I_p, \quad (4a)$$

$$I_c^{obs} = (A_{c,c}A_{c,a}I_c + \beta A_{a,c}A_{a,a}I_a + (1-\beta)A_{a,a}I_a)\cdot I_p, \quad (4b)$$

$$I_a^{obs} = A_{a,a}I_a\cdot I_p, \quad (4c)$$

where the arguments (E, θ) are dropped from all quantities and β is the fraction of air-scattered photons passing through the capillary tube. In these expressions the combined absorption factor ($A_{s,c+s+a}$ or $A_{c,c+s+a}$) has been approximated by the product of three absorption factors ($A_{s,c}A_{s,s}A_{s,a}$ or $A_{c,c}A_{c,s}A_{c,a}$). Factoring by $A_{s,a}$ or $A_{c,a}$ is justified because the absorption by air is mainly determined by the length from the scattering volume to the detector, and almost independent of the coordinates of the scattering point. Factoring by $A_{s,c}$ or $A_{c,c}$, however, is only justified because of the thinness of the cell wall.

Since I_a is a small quantity, β and the difference in the scattering volume of air in Eqs. 4a, 4b, and 4c are ignored, and the relation

$$I_s = \frac{(I_s^{obs} - I_a^{obs}) - A_{c,s}(I_c^{obs} - I_a^{obs})}{A_{s,s}A_{s,c}A_{s,a}\cdot I_p} \quad (5)$$

is obtained. Since $A_{s,a}$ and $A_{a,a}$ are safely assumed to be equal, $A_{a,a}I_p$ ($=A_{s,a}I_p$) is determined from the scattering intensity of air by using the theoretical value of I_a.[14] Thus, Eq. 5 gives I_s by using the calculated values of $A_{s,s}$, $A_{c,s}$, and $A_{s,c}$.

The procedure for obtaining the coherent intensity per molecule (I_{coh}) from I_s by connecting the data from different scattering angles was described previously.[10] The coherent and incoherent atomic scattering factors were taken from tables.[15] The obtained I_{coh} is shown by the broken curve in Fig. 7.

Structure Determination

The interatomic distances and the vibrational amplitudes of a liquid chloroform molecule were assumed to be equivalent to those in the gas phase, which were found in the literature,[16,17] and are listed in Table 1. By using these parameters, the intensity of the intramolecular interference was calculated and subtracted from the total coherent intensity (I_{coh}) to give the intermolecular intensity (I_{inter}) shown in Fig. 7.

By subtracting the self-scattering intensity from I_{inter} and multiplying a modification function,[18]

$$M(s) = \left(\sum_{\alpha} f_{\alpha}(s)\right)^{-2}, \quad (6)$$

where $f_\alpha(s)$ are the atomic scattering factors, the total structure function ($i(s)$) was obtained. The Fourier transform of the s-weighted structure function ($si(s)$) has led to a difference radial distribution function, as shown in Fig. 8. Beyond $r = 9$ Å peaks of the radial distribution appear at almost equal intervals, i.e., 5.4 Å. Therefore, a simple quasi-crystalline model with a molecular arrangement of 5.4 Å intervals was searched. A bcc (body-centered cubic) model and a fcc (face-centered cubic) model were compared, as shown in Table 2; the former was found to be more suitable because the positions of both the first and second peak were consistent with the observed peak positions of the liquid. According to the theory of reciprocal-space expansion,[1,19] it has been shown that the positions of distinct peaks of liquids at smaller s region should be coincident with the peak positions of the powder pattern of the same lattice structure as that of the underlying local lattice of the liquid. Moreover, the number density of the bcc model, namely, two in a cube of $a = 6.24$ Å, is close to the bulk density (1.9) in the same cube at 15 °C or 1.489 g cm^{-3}. It should be noted, however, that the number density does not reject the fcc model, since four in a cube of 7.61 Å is equivalent to 2.15 in a cube of the bcc model.

The crystal structure of chloroform was reported by Fourme and Renaud.[20] The powder-diffraction pattern was simulated with their structure by using the RIETAN program for a Rietvelt analysis,[21] and compared with the observed intermolecular intensities of the liquid in Fig. 9. Evidently there is no correspondence with each other, especially in the region $s < 2.5$ Å^{-1}. The quasi-crystalline model of the liquid should be rather different from the structure of its crystalline

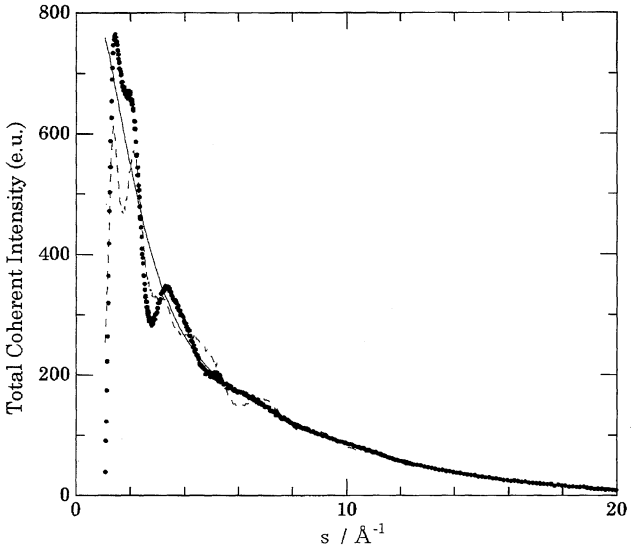

Fig. 7. Intermolecular coherent intensity I_{inter}.
Thin solid line shows the self-scattering and broken curve is I_{coh} including the intramolecular contributions.

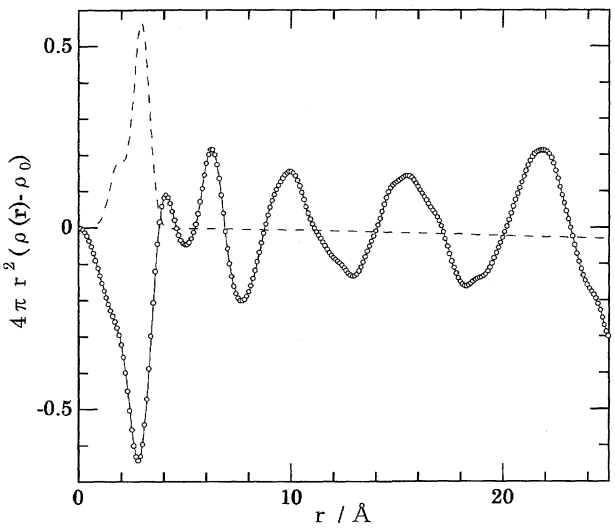

Fig. 8. Intermolecular difference radial distribution function of chloroform.
The broken curve shows the intramolecular distribution.

Table 1. Distances r and Root-Mean-Square Amplitudes l of Gaseous Chloroform

	r/Å[a]	l/Å[b]
C–Cl	1.752	0.0524
Cl···Cl	2.901	0.0691

a) Ref. 16. b) Ref. 17.

Table 2. Comparison of Peak Positions (in Å^{-1})

Liquid (obs)	bcc ($a = 6.24$ Å)	fcc ($a = 7.61$ Å)
1.44	(110) 1.43	(111) 1.42
2.00	(200) 2.01	(200) 1.65
	(211) 2.47	(220) 2.33

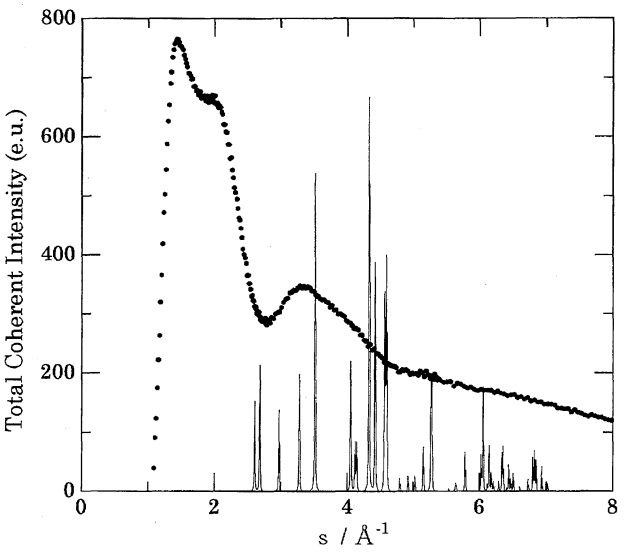

Fig. 9. Comparison of I_{inter} for chloroform with simulated powder pattern of crystalline phase.

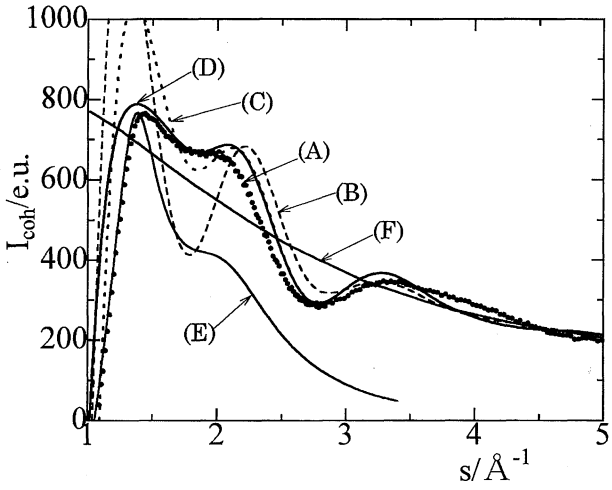

Fig. 10. Calculated intensity functions as compared with the observed I_{inter}(A). (B) Up to the second nearest neighbors (15 molecules); (C) 34% of the nearest neighbors in (B) have been replaced by the super-near configurations; (D) Curve (C) plus the contribution of the continuous region; (E) Calculated by the reciprocal-space expansion; (F) The self-scattering intensities.

phase.

Simulations of the intensity based on a model were performed by both a real-space expansion[22] and by a reciprocal-space expansion.[1,19] The expressions given in Refs. 1, 19, and 22 were modified so that the terms for the intramolecular interference were subtracted. The mean-square deviation of distance r was given by the Prins relation,[3] $l^2 = 2Dr$, where D is the Prins parameter. The scattering intensities from hydrogen atoms were neglected.

By adopting the bcc-like model with the assumption that the molecular C_3-axes were along one of the body-diagonals, four different arrangements of two molecules in the unit cell were examined by the reciprocal-space expansion: (1) C–H bonds towards the same direction and C–Cl bonds are eclipsed, (2) C–H as in (1) and C–Cl's staggered, (3) C–H bonds are directed oppositely and C–Cl's eclipsed, and (4) C–H as in (3) and C–Cl's staggered. Arrangement (2) was found to be the best representative of the observed intensity function. The deviation of the C_3-axis of one of the two molecules from body-diagonal up to 20° was tested, and no remarkable change in the intensity was found. Thus, no deviation was assumed.

The orientation of the C–Cl bonds relative to the unit-cell axes was examined in two extreme cases: (a) one C–Cl bond is in the plane defined by the body-diagonal and the c-axis and (b) the C–Cl bonds are rotated by 90° from the direction of (a) around the C_3-axis. The intensity function calculated by the real-space expansion was, in case (a), out of phase from the observed interference pattern in the region $s = 2$—3 Å^{-1}, while in case (b) it was in general agreement with the observation. Thus, the unit-cell structure was defined as case (b). Since the two molecules in the unit cell are in a staggered configuration with respect to the C–Cl bonds, the symmetry of the unit cell is not exactly bcc, but of the CsCl type.

By using up to the second nearest neighbors (15 molecules including the central one) and the Prins parameter $D = 0.04$ Å, this model has given the intensity curve (B) shown in Fig. 10.

The discrepancy in the region $s = 1.7$—3 Å^{-1} indicates some defects in the present model, although that around the first peak may be eliminated by adding the contribution of the continuous region. In the distribution of the Cl···Cl distances of the present model, the number of distances longer than 5 Å is three-times as many as that of distances shorter than 5 Å. In considering that there is a distinct peak around 4 Å in the radial distribution of Fig. 8, it seems that the inclusion of additional shorter distances would improve the model.

Two configurations in which molecules are closer than in the nearest-neighbor configuration of the bcc-like model were considered: (a) a staggered configuration, which had already existed in the bcc-like model, namely, along one of the body diagonal, with a shorter C···C distance of 3.9 Å instead of 5.4 Å; and (b) the configuration found in the crystal,[20] the coordinates being given in Table 3. This configuration is not the shortest with respect to the C···C distance, but includes the shortest Cl···Cl distance. In these super-near configurations the Prins parameter was set to be smaller, namely,

Table 3. Super-Near Configuration in the Crystal[a]

		x/a	y/b	z/c
Molecule 1	C	0.09	0.25	0.473
	Cl1	0.1892	0.0995	0.358
	Cl1′	0.1892	0.4005	0.358
	Cl2	0.1072	0.25	0.772
Molecule 2	C	0.59	0.25	1.027
	Cl1	0.6892	0.0995	1.142
	Cl1′	0.6892	0.4005	1.142
	Cl2	0.6072	0.25	0.728

a) Orthorhombic: $a = 7.485$ Å, $b = 9.497$ Å, $c = 5.841$ Å, see Ref. 20.

Table 4. Reciprocal Lattice Vectors

Indices	b_ν/Å^{-1} a)	n_ν b)	Intensity
100	1.01	6	Negligible
110	1.42	12	Strong
111	1.75	8	Weak
200	2.02	6	Weak
210	2.26	24	Medium
211	2.47	24	Medium
220	2.84	12	Negligible
221	3.03	24	Weak
222	3.50	8	Negligible

a) Length of the reciprocal lattice vector. b) Number of the reciprocal lattice points with the same b_ν.

at $D = 0.012$ Å. By replacing 17% of the nearest neighbors by the super-near configuration (a) and another 17% by (b), the intensity curve (C) shown in Fig. 10 was obtained. The contribution of the continuous region was added by Eq. 7 of Ref. 22 and the upper solid curve (D) was obtained with $R_c = 6.5$ Å and $l_c = 1.1$ Å; R_c is the range beyond which the distribution is regarded as being continuous and l_c is the damping parameter due to an ambiguity of the R_c value.

The lower solid curve (E) in Fig. 10 was calculated by a reciprocal-space expansion[1,19] with $D = 0.12$ Å and the reciprocal lattice vectors up to 222, as shown in Table 4. Among them, the contributions from 110, 111, 200, 210, 211, and 221 were substantial. Those from 100, 220, and 222 were negligible. Each set of indices represents all of the reciprocal lattice points that can be reached by permutation and a change of sign of the indices. The numbers of such points are shown as n_ν in Table 4.

Discussion and Conclusion

According to the results so far mentioned, the structure of liquid chloroform is characterized by its rapid loss of positional and orientational correlations as the distance between the molecules increases. The correlation is rather strong for the super-near configuration ($D = 0.012$ Å), and moderate up to the second nearest neighbors with a D value of 0.04 Å, which is nearly the same as that in the case of carbon tetrachloride, and is rapidly lost. In the real-space expansion, a continuous distribution beyond 6.5 Å is a suitable description, and in the reciprocal space expansion a large D value (0.12 Å) is used for expressing the long-range structure of the liquid. The structure is much less ordered than that of carbon tetrachloride.[22]

As for the nearest-neighbor configurations, the alignments of the molecular C_3-axes in the present model are rather parallel, including that in the super-near configuration found in the crystal. The orientational correlation function studied by Bertagnolli et al.[8] suggests that the molecular C_3-axes are rather mutually antiparallel. The angles between the molecular C_3-axis and the intermolecular center-center line are 0, 180, 71, 119° in the bcc-like model and 42 and 138° in the crystalline super-near configuration. Some of these angles are outside the ranges 0—55° and 125—180° given in Ref. 8. The number of nearest neighbors in Ref. 8 is six in discordance with eight of the present model, although the nearest-neighbor distance (4.8 Å) is approximately coincident with the average of the nearest-neighbor distances (5.1 Å) in the present model. The consistency of the present model with that implied by the orientational correlation study of Ref. 8 is not very satisfactory, and much is left for future studies.

It may be said that the degradation of molecular symmetry from T_d of carbon tetrachloride to C_{3v} of chloroform, accompanied by the participation of a dipole–dipole interaction, has brought about much more complication concerning the structure of the liquid.

References

1) T. Iijima and K. Nishikawa, *J. Mol. Struct.*, **352/353**, 213 (1995), and papers cited therein.
2) A. H. Narten and H. A. Levy, *Science*, **165**, 447 (1969).
3) J. A. Prins and H. Peterson, *Physica*, **3**, 147 (1936).
4) K. Nishikawa and N. Kitagawa, *Bull. Chem. Soc. Jpn.*, **53**, 2804 (1980).
5) H. H. Paalman and C. J. Pings, *J. Appl. Phys.*, **33**, 2635 (1962).
6) H. Bertagnolli, D. O. Leicht, and M. D. Zeidler, *Mol. Phys.*, **35**, 193 (1978).
7) H. Bertagnolli, D. O. Leicht, M. D. Zeidler, and P. Chieux, *Mol. Phys.*, **35**, 199 (1978).
8) H. Bertagnolli, D. O. Leicht, M. D. Zeidler, and P. Chieux, *Mol. Phys.*, **36**, 1769 (1978).
9) Y. Murata and K. Nishikawa, *Bull. Chem. Soc. Jpn.*, **51**, 411 (1978).
10) K. Nishikawa and T. Iijima, *Bull. Chem. Soc. Jpn.*, **57**, 1750 (1984).
11) W. L. Bond, "International Tables for X-Ray Crystallography," D. Reidel, Dordrecht/ Boston/ Lancaster (1985), Vol. II, p. 291.
12) "International Tables for X-Ray Crystallography," D. Reidel, Dordrecht/ Boston/ Lancaster (1985), Vol. III, p. 175.
13) Communicated from Toho Co., Ltd., an agency of Hilgenberg.
14) K. Nishikawa, K. Ishizawa, Y. Kodera, and T. Iijima, *Jpn. J. Appl. Phys.*, **25**, 1431 (1986).
15) "International Tables for X-Ray Crystallography," Kynoch, Birmingham (1974), Vol. IV, pp. 71 and 258.
16) M. Jen and D. R. Lide, Jr., *J. Chem. Phys.*, **36**, 2525 (1962).
17) V. Galasso, G. De Alti, and G. Costa, *Spectrochim. Acta*, **21**, 669 (1965).
18) A. Habenshuss and A. H. Narten, *J. Chem. Phys.*, **92**, 5692 (1990).
19) K. Nishikawa and T. Iijima, *Bull. Chem. Soc. Jpn.*, **59**, 117 (1986).
20) R. Fourme and M. Renaud, *C. R. Acad. Sci. Paris*, **B263**, 69 (1966).
21) F. Izumi, *Nihon Kesshougakkaishi*, **51**, 411 (1978), in Japanese.
22) K. Nishikawa and T. Iijima, *Bull. Chem. Soc. Jpn.*, **58**, 1215 (1985).